

Article

Influence of Continuous Casting Speeds on Cast Microstructure and Mechanical Properties of an ADC14 Alloy

Yoon-Seok Lee ^{1,*}, Yuya Makino ¹, Jun Nitta ¹ and Eunkyung Lee ²

¹ Graduate School of Natural Science and Technology, Okayama University, Okayama 700-0082, Japan; po507fwv@s.okayama-u.ac.jp (Y.M.); p8177t18@s.okayama-u.ac.jp (J.N.)

² Department of Ocean Advanced Materials Convergence Engineering, Korea Maritime and Ocean University, Busan 49112, Korea; elee@kmou.ac.kr

* Correspondence: y_lee@okayama-u.ac.jp; Tel.: +81-80-3332-4770

Received: 31 March 2020; Accepted: 8 May 2020; Published: 11 May 2020



Abstract: To improve the mechanical properties of the casting alloys, various attempts have been made to use alternative casting technologies. The Ohno continuous casting (OCC) process is a unidirectional solidification method, which leads to high-quality cast samples. In this study, the Al-Si-Cu-Mg alloy was cast at casting speeds of 1 mm/s, 2 mm/s, and 3 mm/s, by the OCC process. The aim of this study is to investigate the effects of the casting process parameters, such as casting speeds and cooling conditions, on the crystallization characteristics and mechanical properties of OCC-Al-Si-Cu-Mg alloy. Particularly, secondary dendrite arms spacing of α -Al dendrites in OCC samples significantly decreases with increasing casting speed. Moreover, the mean tensile strength of the samples, produced at the highest casting speed of 4.0 mm/s, is significantly higher than that for the samples produced at a casting speed of 1.0 mm/s.

Keywords: aluminum alloy; casting speed; solidification; Ohno continuous casting; gravity casting; dendritic spacing

1. Introduction

The reductions in automotive exhaust greenhouse gases, such as carbon dioxide (CO₂) and nitrogen oxides (NO_x), are strongly required for environmental reasons. Light-weighting of vehicles presents an opportunity for cutting greenhouse gas emissions. Aluminum (Al) alloys are one of the light weighting automotive materials, which meets vehicle safety and performance requirements [1]. Therefore, automotive parts made of heavy steel have been replaced with Al alloys. Particularly, the hypereutectic Al-Si alloy family is widely used in the automotive industry because of its high strength, good castability, and low density.

The Al-Si-Cu-Mg alloy, used in this study, is particularly the commercial hypereutectic Al-Si₁₆-Cu₄-Mg_{0.6} alloy (JIS (Japanese Industrial Standards) ADC14). This Al-Si-Cu-Mg alloy has been also widely used for various automotive parts, such as linerless engine blocks, pistons, pumps, and compressors. Furthermore, there has been increasing use in the cast Al-Si-Cu-Mg alloy for automotive parts, over the world. The cast Al-Si-Cu-Mg alloy microstructure consists of mainly coarse α -Al, primary silicon (Si), and needle-shaped eutectic phases, which significantly affects the mechanical properties of Al-Si-Cu-Mg alloy [2]. In particular, it should be noted that the mechanical properties of Al-Si-Cu-Mg alloy are also directly affected by α -Al dendrite size, as indicated by dendrite arms spacing (DAS). However, the use of this Al-Si-Cu-Mg alloy, to replace heavy steel in automotive industry, has been restricted because of their lower strength and lower ductility.

Al-Si alloy family has been investigated using a unique continuous casting technique proposed by Ohno, which is known as the Ohno continuous casting (OCC) process. The OCC process is a unidirectional solidification method, and this casting process provides phase control and texture control [3], which can lead to easy control of microstructure size [4] and crystal orientation [5]. Some researchers have investigated the mechanical properties of OCC-Al alloys, showing excellent tensile and fatigue properties. This can be explained by that their unidirectional microstructures, low defect density, and uniformly oriented lattice structure [6–8]. Therefore, it is believed that the OCC process is useful in the automotive industry.

These days, a better understanding of how alloy solidifies at different casting conditions, involving cooling rates is required in order to improve mechanical properties of cast Al-Si-Cu-Mg alloys as automotive parts. However, very little investigation has been reported, which includes the interpretation of cooling conditions and mechanical properties for the OCC-Al-Si-Cu-Mg alloy on a metallurgical basis.

Therefore, the Al-Si-Cu-Mg samples were cast at casting speeds of 1 mm/s, 2 mm/s, 3 mm/s, and 4 mm/s via the OCC process in this study. In addition, the influences of microstructures, such as α -Al phases, primary Si, and DAS on the mechanical properties of cast Al-Si-Cu-Mg alloys were investigated. The aim of this work is to investigate the effects of casting speeds and cooling conditions on the α -Al dendritic grains-growing and tensile properties of OCC-Al-Si-Cu-Mg alloy.

2. Experimental Procedure

2.1. Materials

Table 1 shows the chemical compositions of Al-Si-Cu-Mg alloy used in this study. The Al-Si-Cu-Mg samples were prepared by the OCC process. In this study, the samples were also prepared by the gravity cast (GC) process for comparison with the OCC process. Figure 1a shows a schematic drawing of a horizontal-type OCC arrangement, consisting of a melting furnace, a heated graphite mold with a diameter of 5 mm, a graphite crucible, a cooling device, and a dummy rod for withdrawal of the cast sample. Approximately 0.4 kg of Al-Si-Cu-Mg ingot was placed in the graphite crucible for melting, with the graphite mold heated to approximately 910 K, which is just above the liquidus of the Al-Si-Cu-Mg alloy. The melted Al alloy in the crucible was fed continuously into the mold through a runner. A schematic drawing of conventional GC arrangement, consisting of an electric furnace, a crucible, and a metal mold, is shown in Figure 1b for comparison. The Al-Si-Cu-Mg ingot was also placed and melted in the crucible at approximately 910 K for 1 h, using the electric furnace. Then the molten alloy was solidified in the wide rectangular mold.

To obtain various microstructural characteristics, the casting operation of the OCC process was carried out at different speeds, from 1.0 mm/s to 4.0 mm/s. In this study, the round-rod samples were produced via the OCC process with a diameter of 5 mm and a length of approximately 1 m.

Table 1. Chemical composition (mass%) of the Al-Si-Cu-Mg alloy used in this study.

Alloy \ Element	Cu	Si	Mg	Zn	Fe	Mn	Al
Al-Si-Cu-Mg	4.20	16.49	0.61	0.37	0.72	0.31	bal.

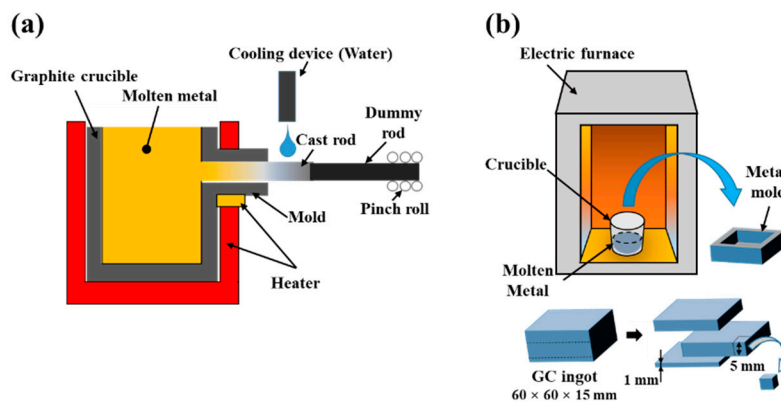


Figure 1. Schematic drawings of (a) vertical Ohno continuous casting (OCC) and (b) gravity cast (GC) process.

2.2. Metallurgical Analysis

Some of the OCC and GC samples were sectioned to observe microstructures using optical microscope (OM). The cut surfaces were first metallographically polished using up to a 4000 grit-sized silicon carbide paper and were subsequently buff-polished using an Al_2O_3 powder with an average diameter of $0.3 \mu\text{m}$ and a colloidal SiO_2 solution.

The DAS were also investigated from optical micrographs of cross-section of the cast samples. In particular, the secondary dendrite arms spacing (SDAS) was determined by several optical micrographs and applying an image analysis software. The total spacing from the first to the last arm in a certain area was firstly measured to calculate the SDAS. Consequently, the SDAS was obtained from the following equation:

$$\text{SDAS} = L / (n \times V), \quad (1)$$

where L is the measuring length in μm , n is the number of existing dendrite arms in a certain area, and V is the micrograph magnification. Then, an average value of the results was calculated after repeated measurements in different areas.

In addition, some of the cast rod was sectioned parallel to the withdrawal direction and scanning electron microscope (SEM)-based electron back-scattered diffraction (EBSD) analysis was performed to develop a more quantitative view of the microstructures. The cut surfaces were also buff-polished and the orientation data obtained from the EBSD scans were analyzed using an Orientation Imaging Microscopy (OIMTM) analysis software (version 7.2, EDAX Inc., Mahwah, NJ, USA). Moreover, after the tensile tests, the fracture surfaces were also observed to analyze the material defects, using SEM.

2.3. Mechanical Properties

The hardness of longitudinal cross-sections of OCC samples was measured using a Vickers hardness tester at a load of 9.8 N for a holding time of 15 s. The hardness of GC samples was also measured under the same conditions. Nine different points were measured for each sample. The highest and lowest values were discarded, and the hardness of each sample was determined using the average of the remaining seven values.

Moreover, the tensile tests were carried out using an electro-servo-hydraulic system with a crosshead speed of 1 mm/min in air at room temperature. Dumbbell-shaped round specimens (4 mm in diameter and 30 mm in length) were used as shown in Figure 2. The three specimens were prepared and tested for each tensile test. Load and strain were measured using a load cell attached to the machine and a foil-type strain gage attached to the gage section of the specimens, respectively. The tensile strength and strain of the specimens were obtained from the tensile stress–strain curve.

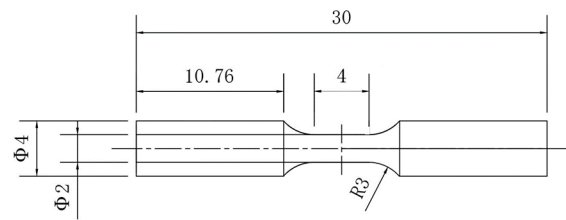


Figure 2. Schematic drawing of specimen used for tensile test.

3. Results

3.1. Microstructural Characteristics

Figure 3 shows optical micrograph of cross-section of sample produced by GC. The microstructure basically consists of large primary Si, embedded between primary α -Al grains. Moreover, Figure 4 shows optical micrographs of cross-sections of OCC samples produced at casting speeds of 1.0, 2.0, 3.0, and 4.0 m/s. The microstructures of OCC samples also consist of large primary Si, embedded between primary α -Al grains. It can be also clearly observed that the mean sizes of primary Si are the largest at a speed of 1.0 mm/s, regardless of the observed location.

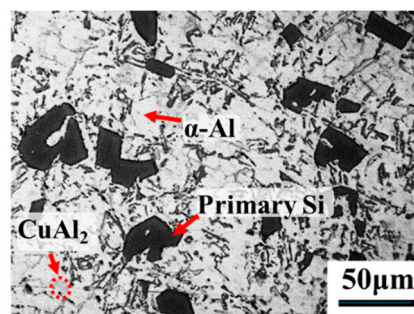


Figure 3. Optical micrograph showing microstructure of GC sample.

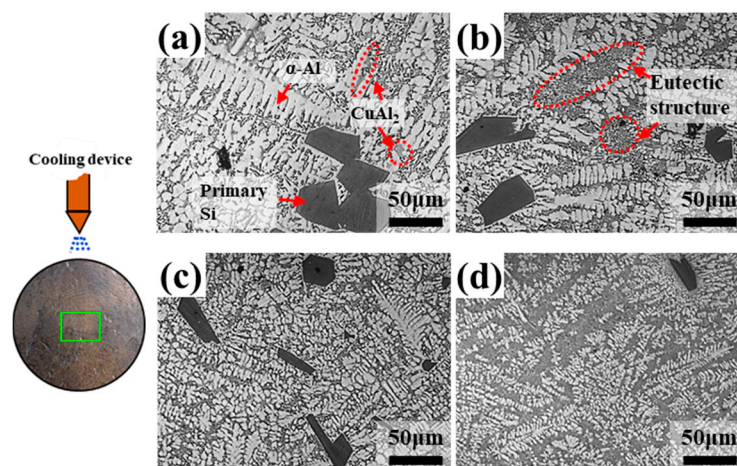


Figure 4. Optical micrographs of cross-sections of OCC samples; middle parts cast at speeds of (a) 1.0 mm/s, (b) 2.0 mm/s, (c) 3.0 mm/s, and (d) 4.0 mm/s.

Figure 4 shows middle parts of cross-sectioned OCC samples. In this study, no sharp difference is observed between upper and lower parts of the samples at any of the casting speeds, although upper parts were cooled directly by spray water and cooled at the fastest rate (Figure 1a). It can be explained by that the diameter of cast rod is too small to show large difference in the cooling rate, between upper and lower parts.

Moreover, it is observed that the grain structure transition occurs with increasing casting speeds, owing to the different cooling rates. The morphologies of primary Si phases show sharp edges and flat faces, indicating the facet characteristics. Furthermore, the distributions of primary Si phases are non-homogenous, regardless of the casting speeds. In particular, both the sizes and amount of primary Si are reduced between 1.0 mm/s and 2.0 mm/s. Larger primary Si particles (approximately 5–100 μm in equivalent diameter) are observed in the samples cast at a lowest speed (1.0 mm/s), while smaller primary Si particles (approximately 5–40 μm in equivalent diameter) are observed at the other speeds (2.0 mm/s, 3.0 mm/s, and 4.0 mm/s).

In addition, optical micrographs of longitudinal cross-sections are also shown in Figure 5. It is clear from the results at higher casting speeds (Figure 5b–d) that the α -Al dendrite cells grow in the withdrawal direction. No sharp difference was also observed between upper and lower parts of cast samples, regardless of the casting speeds. The grain structure transition is also observed in longitudinal cross-sections with changes in casting speeds. The quantitative analysis of dendritic structures can be conducted by measurements of DAS. As shown in Figure 5, it is clearly observed that the dendritic structures are refined with increasing casting speed. It is considered that higher cooling rates during solidification induce a higher degree of refinement in dendritic array.

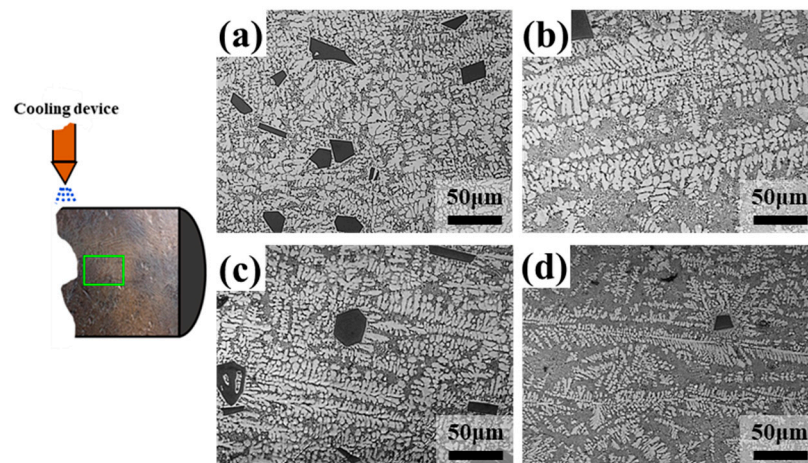


Figure 5. Optical micrographs of longitudinal cross-sections of OCC samples; middle parts cast at speeds of (a) 1.0 mm/s, (b) 2.0 mm/s, (c) 3.0 mm/s, and (d) 4.0 mm/s.

EBSD analysis was also carried out in order to analyze morphologies of the dendritic structures, including SDAS. All observations were obtained from longitudinal cross-sections of the samples as shown in Figure 6. It can be more clearly observed from both image quality (IQ) maps and corresponding grain boundary (GB) maps that SDAS of α -Al dendrites significantly decreases with increasing casting speed. SDAS is one of the most important factor, which affects the mechanical properties of Al-Si alloy family. The effects of SDAS and grain size on mechanical properties are similarly obtained for the related Al-Si alloys [9]. Figure 7 shows the relationship between the casting speeds and SDAS. SDAS of α -Al dendrites in OCC samples significantly decreases with increasing casting speed. Moreover, SDAS of OCC samples is smaller than that in GC samples, regardless of the casting speed. The mean SDAS is approximately 4.0 μm for the high casting speed of 4.0 mm/s and 8.7 μm for the low casting speed of 1.0 mm/s, resulting from the longitudinal cross-sections. It is considered that the changes in SDAS are due to a different cooling rate, which lead to different solidification behavior.

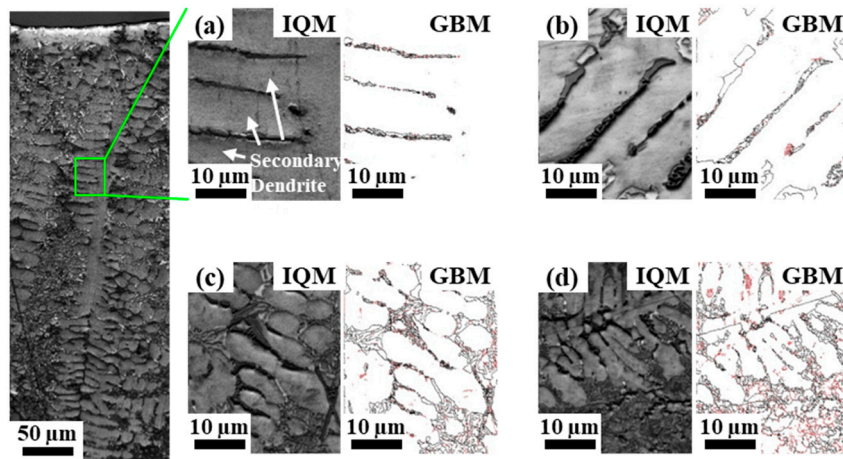


Figure 6. Electron back-scattered diffraction (EBSD) analysis of longitudinal cross-sections of OCC samples: image quality (IQ) maps and corresponding grain boundary (GB) maps of samples cast at speeds of (a) 1 mm/s, (b) 2 mm/s, (c) 3 mm/s, and (d) 4 mm/s.

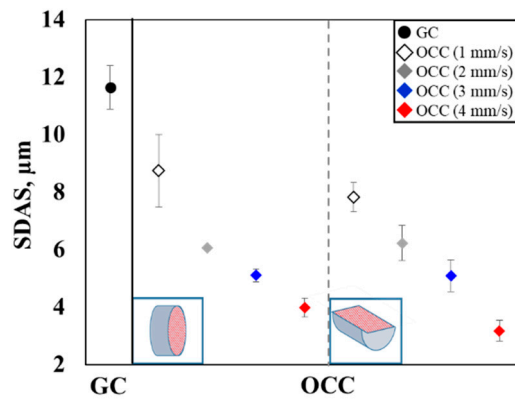


Figure 7. Secondary dendrite arms spacing (SDAS) of GC and OCC samples.

As shown in Figure 8, the cooling rates (CR) of the casting samples were also estimated from the following equation [10]:

$$CR = 2 \times 10^4 \times SDAS^{-2.67} \tag{2}$$

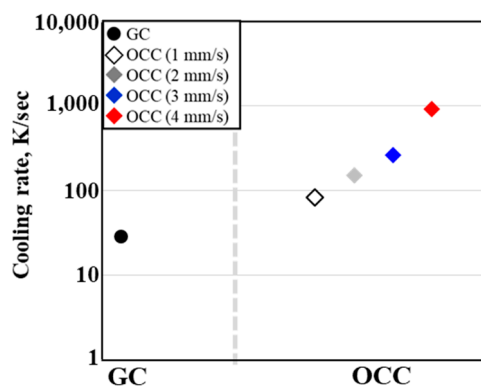


Figure 8. Relationship between casting rate and cooling rate for Al-Si-Cu-Mg alloys.

The cooling rates significantly increase with increasing casting speeds for OCC samples. Furthermore, the estimated cooling rates of OCC samples are higher than those of GC samples, regardless of the casting speed. It can be explained by that OCC samples have much smaller volumes with cooled directly with sprayed water.

3.2. Mechanical Properties

As shown in Figure 9, it is clearly observed that the hardness of OCC samples significantly increases with increasing casting speeds, showing similar behaviors with those of CR plotted in Figure 8. Grain boundaries generally act as barriers to dislocation motion. As mentioned in Section 3.1, the effects of SDAS and grain size on mechanical properties are similar for the Al-Si-Cu-Mg alloy. Consequently, it is considered that the refinement of SDAS, with increasing cooling rate, leads to increase in hardness. Moreover, the mean hardness of OCC samples cast at speeds over 3 mm/s exceeds that of GC sample.

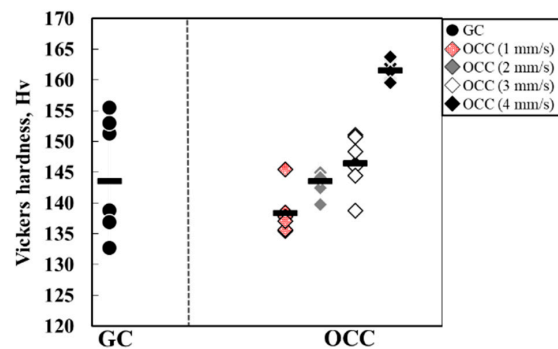


Figure 9. Vickers hardness of GC and OCC samples.

In addition, Figure 10 shows the variations of ultimate tensile strength as functions of casting speeds. It can be observed that the mean ultimate tensile strength increases at higher casting speeds. These results from the tensile tests are similar to the hardness results shown in Figure 9. The mean tensile strength shows a maximum for the samples produced at the highest casting speed of 4.0 mm/s, which is about 70% higher than that for the samples produced at a casting speed of 1.0 mm/s. Moreover, the mean tensile strength of OCC samples cast at 4.0 mm/s is also much higher (by more than 2 times) than that of the GC samples.

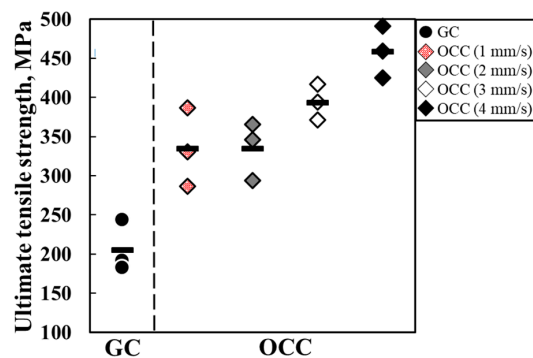


Figure 10. Ultimate tensile strength of GC and OCC samples.

The variations of fracture strain as functions of casting speeds are also shown in Figure 11. No sharp difference is observed with a changing casting speed. Nevertheless, the fracture strains of OCC samples are slightly higher compared to that of GC samples, regardless of the casting speeds.

It is believed that such improvements of mechanical properties of OCC samples can be explained by the presence of unidirectional microstructures and refined dendritic array. Particularly, the improvements of the tensile strength of OCC samples are owing to the refinement of SDAS, which may be the obstacles to the movement of dislocations. SDAS is particularly a significant factor determining the mechanical properties of cast Al-Si-Cu-Mg alloys due to grain-boundary hardening, although the mechanical properties are also affected by other microstructural characteristics, such as eutectic and Si phases.

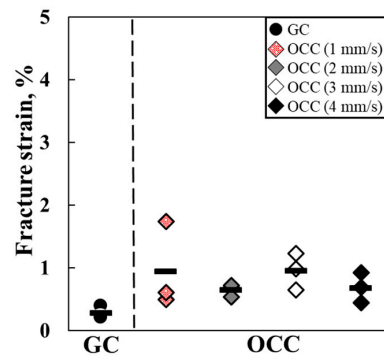


Figure 11. Fracture strain of GC and OCC samples.

SEM fractographs of the tensile specimens cast by GC and OCC are shown in Figure 12. Large pores (approximately 150 μm in diameter) can be observed only at the fracture surface of GC samples, as shown in Figure 12a. On the other hand, from the microstructural observations, the fine casting defects (pores or inclusions) are detected in all of OCC samples. The casting defects could give rise to the stress concentration, leading to the crack formation during the tensile test [11]. It should be noted that the large pore, among the casting defects, is the most responsible for crack formation. Hydrogen (H), as the only gas capable of dissolving to significant quantities in an aluminum melt, is the main factor influencing gas porosity. It is considered that the large pore of GC sample is generated by H gas during the solidification in this study. This is because the morphology of the large pore on the fracture surface does not seem to be a shrinkage pore with an irregular shape, but a gas pore of a spherical shape [11]. It is considered that the large gas pore in the GC sample is generated by the slower cooling rate compared to the OCC samples. Furthermore, not only SDAS, but also the casting defects are smaller and better distributed at a higher casting speed. Consequently, the lower strength and ductility of GC alloys are assumed to result from not only enlarged $\alpha\text{-Al}$ and SDAS but also internal defects in this study.

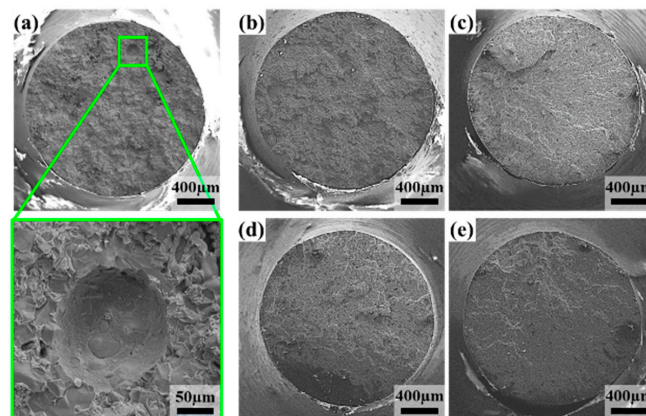


Figure 12. SEM fractographs of Al-Si-Cu-Mg samples cast by (a) GC and OCC at casting speeds of (b) 1.0 m/s, (c) 2.0 m/s, (d) 3.0 m/s, and (e) 4.0 m/s, after tensile tests.

4. Summary

In this study, the effects of casting speeds and cooling conditions on the cast microstructures and mechanical properties of Al-Si-Cu-Mg alloy were investigated. The primary findings of this study are the following:

- 1) The microstructures, particularly those of the sizes of $\alpha\text{-Al}$ grains, differ among the samples, which resulted from the different cooling rate. SDAS of $\alpha\text{-Al}$ dendrites in OCC samples significantly

decreases with increasing casting speed. Moreover, SDAS of α -Al dendrites in OCC samples is smaller than that in GC samples, regardless of the casting speed.

- 2) The improvements of mechanical properties of OCC samples are owing to the refinement of SDAS, which may be the obstacles to the movement of dislocations. The mean tensile strength shows maximum for the samples produced at the highest casting speed of 4.0 mm/s.
- 3) The large pore can be observed only at the fracture surface of GC samples. On the other hand, only fine casting defects are detected in any of OCC samples. It is believed that the presence of large pores may lead to crack formation during the tensile test.
- 4) The solidification conditions in continuous casting process, leading to the refinement of the dendritic structures and low porosity, are regarded as contributing to the higher quality of the products and mechanical properties of Al-Si-Cu-Mg casting alloy.

Author Contributions: Conceptualization, Y.-S.L.; methodology, Y.-S.L.; formal analysis, Y.-S.L. and Y.M.; investigation, Y.M. and J.N.; resources, Y.-S.L.; data curation, Y.-S.L. and Y.M.; writing—original draft preparation, Y.-S.L.; writing—review and editing, Y.-S.L. and E.L.; visualization, Y.-S.L.; supervision, Y.-S.L.; project administration, Y.-S.L. All authors have read and agreed to the published version of the manuscript.

Funding: This research received no external funding.

Acknowledgments: This work was supported in part by The Light Metal Educational Foundation, Inc., Japan.

Conflicts of Interest: The authors declare no conflict of interest.

References

1. Kim, H.-J.; Keoleian, G.A.; Skerlos, S.J. Economic assessment of greenhouse gas emissions reduction by vehicle lightweighting using aluminum and high-strength steel. *J. Ind. Ecol.* **2011**, *15*, 64–80. [[CrossRef](#)]
2. Okayasu, M.; Takeuchi, S.; Shiraishi, T. Crystallisation characteristics of primary silicon particles in cast hypereutectic Al–Si alloy. *Int. J. Cast Met. Res.* **2013**, *26*, 105–113. [[CrossRef](#)]
3. Soda, H.; Motoyasu, G.; Mclean, A.; Jen, C.K.; Lisboa, O. Method for continuous casting of metal wire and tube containing optical fibre. *Mater. Sci. Technol.* **1995**, *11*, 1169–1173. [[CrossRef](#)]
4. Sengupta, S.; Soda, H.; Mclean, A. Microstructure and properties of a bismuth-indium-tin eutectic alloy. *Mater. Sci.* **2002**, *37*, 1747–1758. [[CrossRef](#)]
5. Okayasu, M.; Ota, K.; Takeuchi, S.; Ohfuji, H.; Shiraishi, T. Influence of microstructural characteristics on mechanical properties of ADC12 aluminum alloy. *Mater. Sci. Eng. A* **2014**, *592*, 189–200. [[CrossRef](#)]
6. Wang, Y.; Huang, H.-Y.; Xie, J.-X. Enhanced room-temperature tensile ductility of columnar-grained polycrystalline Cu–12 wt.% Al alloy through texture control by Ohno continuous casting process. *Mater. Lett.* **2011**, *65*, 1123–1126. [[CrossRef](#)]
7. Okayasu, M.; Yoshie, S. Mechanical properties of Al–Si₁₃–Ni_{1.4}–Mg_{1.4}–Cu₁ alloys produced by the Ohno continuous casting process. *Sci. Eng. A* **2010**, *527A*, 3120–3126. [[CrossRef](#)]
8. Okayasu, M.; Takasu, S.; Yoshie, S. Microstructure and material properties of an Al–Cu alloy provided by the Ohno continuous casting technique. *J. Mater. Process. Technol.* **2010**, *210*, 1529–1535. [[CrossRef](#)]
9. Ceschini, L.; Morri, A.; Gamberini, A.; Messieri, S. Correlation between ultimate tensile strength and solidification microstructure for the sand cast A357 aluminium alloy. *Mater. Des.* **2009**, *30*, 4525–4531. [[CrossRef](#)]
10. Okayasu, M.; Ohkura, Y.; Takeuchi, S.; Takasu, S.; Ohfuji, H.; Shiraishi, T. A study of the mechanical properties of an Al–Si–Cu alloy (ADC12) produced by various casting processes. *Mater. Sci. Eng. A* **2012**, *543*, 185–192. [[CrossRef](#)]
11. Teng, X.; Mae, H.; Bai, Y.; Wierzbicki, T. Pore size and fracture ductility of aluminum low pressure die casting. *Eng. Fract. Mech.* **2009**, *76*, 983–996. [[CrossRef](#)]

